

Optical signatures of quantum delocalization over extended domains in photosynthetic membranes

Christopher A. Schroeder*, Felipe Caycedo-Soler*, Susana F. Huelga, Martin B. Plenio

* These authors contributed equally and

Institute of Theoretical Physics Albert-Einstein-Allee 11 D - 89069 Ulm, Germany

The prospect of coherent dynamics and excitonic delocalization across several light-harvesting structures in photosynthetic membranes is of considerable interest, but challenging to explore experimentally. Here we demonstrate theoretically that the excitonic delocalization across extended domains involving several light-harvesting complexes can lead to unambiguous signatures in the optical response, specifically, linear absorption spectra. We characterize, under experimentally established conditions of molecular assembly and protein-induced inhomogeneities, the optical absorption in these arrays from polarized and unpolarized excitation, and demonstrate that it can be used as a diagnostic tool to determine the coherent coupling among iso-energetic light-harvesting structures. The knowledge of these couplings would then provide further insight into the dynamical properties of transfer, such as facilitating the accurate determination of Förster rates.

I. INTRODUCTION

Nature has evolved a variety of photosynthetic architectures. A detailed, quantitative understanding of the principles that underly their function could assist the design of future energy conversion devices. A wealth of careful structural and spectral studies^{1–6} complemented by first principle calculations^{7–10} have contributed to our current understanding of exciton transfer dynamics in light-harvesting (LH) antenna and reaction center (RC) pigment-protein complexes. Recently, interest in this topic has intensified due to observations of persistent oscillatory features in non-linear optical experiments^{11–17}, which have been reproduced in various LH structures. This has motivated work which reevaluates the nature of the interaction between excitonic dynamics and vibrational motion^{18–20}.

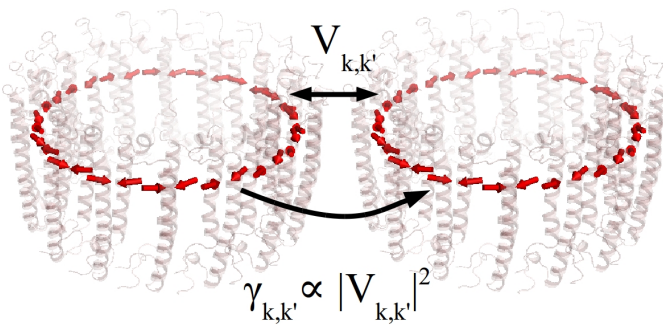


FIG. 1. The Q_y transition dipole moments (red arrows) of the BChl pigments and the protein scaffold (light red) of the LH1 complex in *R. rubrum*, according to a homology model, are pictured schematically²¹. The rate of incoherent energy transfer between excitons k and k' on different LH complexes, $\gamma_{k,k'}$, is determined by the coherent coupling $V_{k,k'}$, as explained in the main text.

Recent work has examined excitonic delocalization restricted to closely-packed pigments in single LH units^{8,22,23}. This approximation is valid for studies of inter-complex energy transfer and fluorescence, which

take place on time scales (\sim ps–ns) much longer than the dephasing (\sim 100 fs), which reduces the excitons to localized (single-unit) domains^{10,24,25}. However, for processes that are faster than dephasing, such as absorption, extended delocalization across LH complexes must be taken into account in an accurate description²⁶. Here, we propose and characterize theoretically an experimental scheme, based on simple linear absorption measurements, which quantifies the coherent coupling among LH complexes in purple bacteria. Based on firm theoretical analysis, we show how this information facilitates the determination of incoherent excitonic transfer rates in systems where the donor fluorescence and acceptor absorption overlap.

II. MATERIALS AND METHODS

Purple bacteria. Photosynthetic membranes of purple bacteria are composed, in general, of well-ordered two-dimensional arrays of LH1 and LH2 complexes, which are responsible for the absorption of light and the subsequent transport of excitation energy to RC pigments, where charge separation drives metabolism under photosynthetic growth conditions^{2–4,6,27–31}. In such membranes, excitonic energy transfer among LH1 and LH2 units has been characterised in terms of incoherent (thermal) hopping³². However, for a description of absorption, which occurs on timescales much shorter than inter-complex energy transfer and dephasing, excitonic delocalization across several harvesting complexes may become relevant. In this work, we analyse excitonic delocalisation across many LH complexes. We will show that this delocalization leads to a redistribution of absorption intensity which is experimentally accessible by exploiting the symmetry of LH1 and LH2 complexes.

For concreteness, we develop our analysis using the LH1 of *R. rubrum*, whose assumed homology of LH1 to LH2 harvesting units permits a straightforward generalization to membranes composed of either complex. The available X-ray structure of the LH1 complex from *Tch.*

*tepidum*³³ and vanishing fluorescence anisotropy of LH1s in *R. rubrum*³⁴ provide support for a closed ring structure with dimeric repeating units of $2N = 32$ bacteriochlorophyll (BChl) pigments in a C_{16} -fold symmetry, as depicted schematically in Figure 1. LH1 complexes from *R. rubrum* naturally aggregate via protein domain-mediated interactions into arrays with a tetragonal packing². In *R. sphaeroides*, LH1 complexes tend to dimerize^{2–4}.

Exciton formalism. Excitonic properties of membranes subject to low-intensity illumination can be obtained from the electronic Hamiltonian in the single excitation subspace:

$$\mathcal{H} = \sum_m \epsilon_m |m\rangle \langle m| + \sum_{m,n} J_{mn} |n\rangle \langle m| \quad (1)$$

where ϵ_m is the excitation energy of pigment m and J_{nm} is the coupling, through the Coulomb exchange mechanism, between the Q_y induced transition dipoles of the electronic excited states $|n\rangle$ and $|m\rangle$ on pigments n and m ³⁵. Diagonalization of \mathcal{H} leads to eigenstates (excitons) $|\alpha\rangle = \sum_n c_n^\alpha |n\rangle$ which are delocalized, in the absence of protein-induced inhomogeneities, over the complete array due to the nearly isoenergetic landscape ($\epsilon_n \approx \epsilon$). These excitons have associated dipole moments, $\vec{D}_\alpha = \sum_n c_n^\alpha \vec{d}_n$, which are linear combinations of the BChl individual dipole moments, $\vec{d}_n = d \hat{d}_n$, and determine the optical response to a polarized incident field with polarization unit vector \hat{E} , which is proportional to the dipole strength $|\vec{D}_\alpha \cdot \hat{E}|^2$.

Excitons are affected by the interactions with the protein environment, which induce quasi-static fluctuations (inhomogeneous broadening) of the excitation energy and the Coulomb coupling in \mathcal{H} and dynamically degrade electronic coherence properties within the excitation lifetime (homogeneous broadening). The dominance of inhomogeneous or homogeneous broadenings in the absorption spectrum can be determined from the specific details of the absorption profile, namely the lineshape function. Purple bacteria antenna complexes at low temperatures are well-modelled by dominantly inhomogeneous broadening^{24,36}, while at higher temperatures, observations support a major contribution from homogeneous mechanisms^{26,37–40}. Accordingly, we simulate the inhomogeneous distributions of pigment energies and coupling strengths by sampling Gaussian distributions with standard deviations of 80 cm^{-1} and 60 cm^{-1} , respectively. The homogeneous width is 465 cm^{-1} such that the full width corresponds to experimentally measured spectra. The influence of larger spectral inhomogeneities is discussed below.

An understanding of the extent of excitonic delocalisation under the influence of protein-induced inhomogeneities is accomplished by appropriate variations of pigment site-energies and couplings. In order to quantify this phenomenon, the usual inverse participation ratio^{9,41}, is generalised to quantify delocalisation *across* rings R of a given exciton α , namely the ring participa-

tion ratio $IPR_R^\alpha = 1 / \sum_{M=1}^R (\sum_{n \in M} |c_n^\alpha|^2)^2$. The IPR_R ranges from 1 to R , and $IPR_R > 1$ unequivocally represents excitonic delocalisation over more than a single ring. The most optically active states, as will be shown shortly, present an appreciable delocalisation length.

III. RESULTS AND DISCUSSION

Extended delocalization. The key prediction of this article is presented in Figure 2(A), which shows that, for different ring assemblies and intermediate values of inhomogeneous disorder, excitonic delocalisation of the most optically-active states will on average extend over several ring structures. This suggests that delocalization must be viewed as a phenomenon occurring in general assemblies of light-harvesting units (with the appropriate packing density of rings). In addition, particular ring assemblies exhibit symmetries which allow the extended delocalization to be verified experimentally, as discussed in the next section.

LD witnesses delocalization and assembly asymmetry. We analyse the consequences of such delocalisation in the polarised and unpolarised optical response in general assemblies. Polarised absorption spectra can be calculated according to

$$\langle A(\phi, \lambda) \rangle \propto \langle \sum_\alpha |\vec{D}_\alpha \cdot \hat{E}(\phi)|^2 f(\lambda - \lambda_\alpha) \rangle \quad (2)$$

where $\langle \dots \rangle$ denotes averages over realisations of disorder and ϕ is the polarization angle of the exciting field. The homogeneous spectral lineshape is determined, in the Markovian limit, by a Lorentzian $f(\lambda - \lambda_\alpha)$, centered at the wavelength λ_α of the corresponding exciton α , and with a width commensurate with the electronic dephasing rate. The linear dichroism (LD)

$$\langle LD(\phi, \lambda) \rangle = \frac{\langle A(\phi, \lambda) \rangle - \langle A(\phi + \pi/2, \lambda) \rangle}{\max\{\langle \langle A(\phi, \lambda) \rangle_\phi \rangle\}} \quad (3)$$

is normalized by the maximum of the unpolarized absorption spectrum, $\langle \langle A(\phi, \lambda) \rangle_\phi \rangle$. For uncoupled LH1 complexes, the circular symmetry leads to an optical response predominantly determined by two orthogonally-polarized degenerate exciton states and vanishing LD^{26,34,42,43}. However, the coherent excitonic interaction among rings may lift such symmetry and result in a finite LD as observed in Figure 2(b).

Notice that not all multiple-ring arrangements present a finite LD, as shown in Figure 2(b). For instance the symmetric square assembly— which presents the greatest IPR_R — has vanishing LD, while the linear array shows a LD with a contrast of $\simeq 4\%$ of the absorption maximum. From these results it is apparent that, although each assembly presents similar delocalization, asymmetric assemblies provide a suitable scenario for the experimental observation of excitonic delocalization using polarized spectroscopy. This point is addressed in more detail in what follows. Consequently, a vanishing LD may

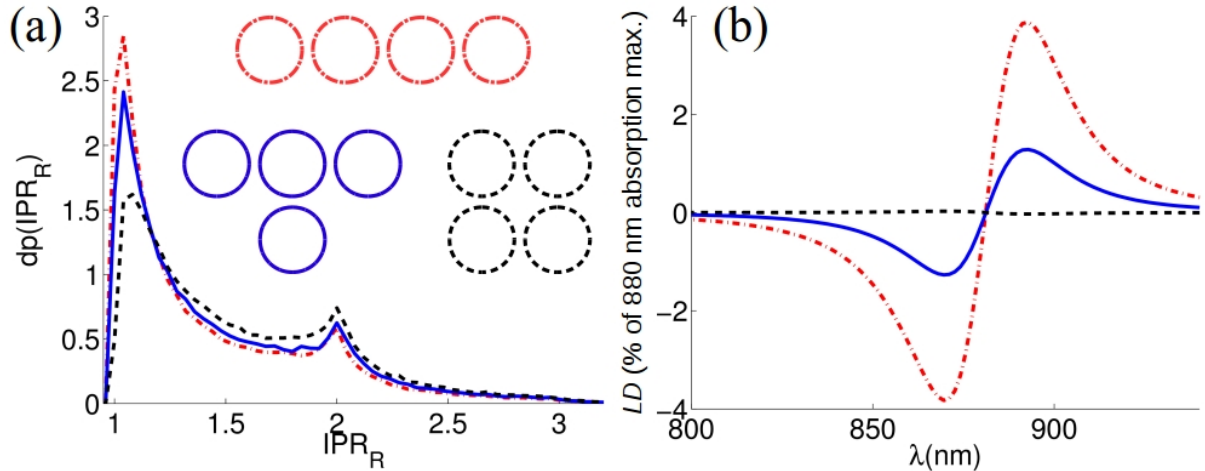


FIG. 2. Extended delocalization across multi-ring arrays in three different configurations (line, T and square). Each four-ring configuration considered in (a) exhibits a similar, although not identical, extent of delocalization, measured by the ring inverse participation ratio IPR_R . Plotted is the probability distribution, $dp(IPR_R)$, of the IPR_R of the exciton state with greatest dipole strength, averaged over realisations of static disorder. The average delocalization length, $\langle IPR_R \rangle$, increases slightly with the number of neighbors, i.e. $\langle IPR_R \rangle = \{1.58, 1.64, 1.71\}$ for the line, T-, and square configurations, respectively. However, the delocalization is witnessed by linear dichroism (LD) only when the assembly exhibits an asymmetry, like in the T and line arrays, as shown in (b).

reflect symmetries of the macro-molecular assembly and does not imply that excitonic delocalisation is restricted to single-ring domains.

Analytical expressions. In order to understand the origin of the asymmetric polarised absorption, an analytical approach is desirable. In the absence of inhomogeneities, the optical response of circular aggregates, resembling LH1 or LH2 rings, is determined by the $|k = \pm 1\rangle = \frac{1}{\sqrt{2N}} \sum_n (-1)^n \exp(2\pi i k \lfloor n/2 \rfloor / N) |n\rangle$ states, where $\lfloor n/2 \rfloor$ is the largest integer smaller than $n/2$. These states carry all the transition dipole moment, namely $\vec{D}_{k=\pm 1} \approx d\sqrt{\frac{N}{2}}(\hat{x} \pm \hat{y})$, where \hat{x} and \hat{y} denote orthonormal axes to be identified with those shown in Figure 3(a). The inter-ring coherent coupling $V_{k,k'} = \langle k, \vec{e} | \mathcal{H} | k', \vec{e}' \rangle$ between excitons k and k' on rings centered at lattice sites \vec{e} and \vec{e}' is much smaller than the energy difference between single-ring excitons, namely $|\langle k, \vec{e} | \mathcal{H} | k, \vec{e} \rangle - \langle k', \vec{e}' | \mathcal{H} | k', \vec{e}' \rangle|$. Such condition results in a minor mixing between states $|k| \neq |k'|$, results in an optical response of assemblies mainly determined by the coupling between the bright $|k = \pm 1, \vec{e}\rangle$ and $|k' = \pm 1, \vec{e}'\rangle$ states from neighbouring rings. In particular for this manifold, it can be shown that $V_{1,1} = V_{-1,-1} < 0$, $V_{1,-1} = V_{-1,1}^*$ and the argument $\arg(V_{1,-1}) = 0$ for $\vec{e} - \vec{e}' = \pm a\hat{x}$ and $\arg(V_{1,-1}) = \pi$ for $\vec{e} - \vec{e}' = \pm a\hat{y}$, where a is the lattice spacing.

In what follows, we consider nearest-neighbor couplings on the square lattice of Figure 3(a), as in Figure 2, as it exhibits the optical signatures of extended delocalization while allowing simple analytical expressions. Qualitatively similar results are obtained for couplings beyond nearest-neighbours and triangular lattices,

which we consider explicitly in the Supporting Information. Rings are centered at lattice sites $\vec{e} = a(q\hat{x} + r\hat{y})$, where $q = 1, \dots, Q \in \mathbb{Z}$, $r = 1, \dots, R \in \mathbb{Z}$ and $a = 120\text{\AA}^3$; single-ring excitons are labeled $|\pm 1, q, r\rangle = |\pm 1, \vec{e}\rangle$. Accordingly, the extended excitonic wavefunctions over the rectangular array read as

$$|\pm, k_q, k_r\rangle = \sqrt{\frac{2 \times 2}{(Q+1)(R+1)}} \times \sum_{q,r} \sin\left(\frac{\pi k_q q}{Q+1}\right) \sin\left(\frac{\pi k_r r}{R+1}\right) |\pm, q, r\rangle \quad (4)$$

where $|\pm\rangle = \frac{1}{2}(|1\rangle \pm | -1\rangle)$ and $k_q = 1, \dots, Q$ and $k_r = 1, \dots, R$ are Fourier quantum numbers corresponding to the \hat{x} and \hat{y} directions, respectively. The optical response is calculated, according to 2, to be

$$\left(\frac{|\vec{D}_{+,k_q,k_r} \cdot \hat{E}(\phi)|^2}{|\vec{D}_{-,k_q,k_r} \cdot \hat{E}(\phi)|^2} \right) \propto \frac{S^2(k_q, Q)}{Q+1} \frac{S^2(k_r, R)}{R+1} \begin{cases} \cos^2 \phi & \text{if } k_q = k_r \\ \sin^2 \phi & \text{if } k_q \neq k_r \end{cases} \quad (5)$$

where the absorption strength is determined by $S(k, W) = \sin\left(\frac{\pi k}{2}\right) \sin\left(\frac{\pi k W}{2(W+1)}\right) \csc\left(\frac{\pi k}{2(W+1)}\right)$ is distributed over states $|\pm\rangle$ along orthogonal polarizations. Given that $S(k, W) \sim \frac{W}{k} \sin^2\left(\frac{\pi k}{2}\right)$ already for $W \gtrsim 3-4$ rings, the dipole strength becomes degradingly small for higher $k > 1$ states, which therefore concentrate dipole moment in the $k_q, k_r = 1$ states in the rectangular con-

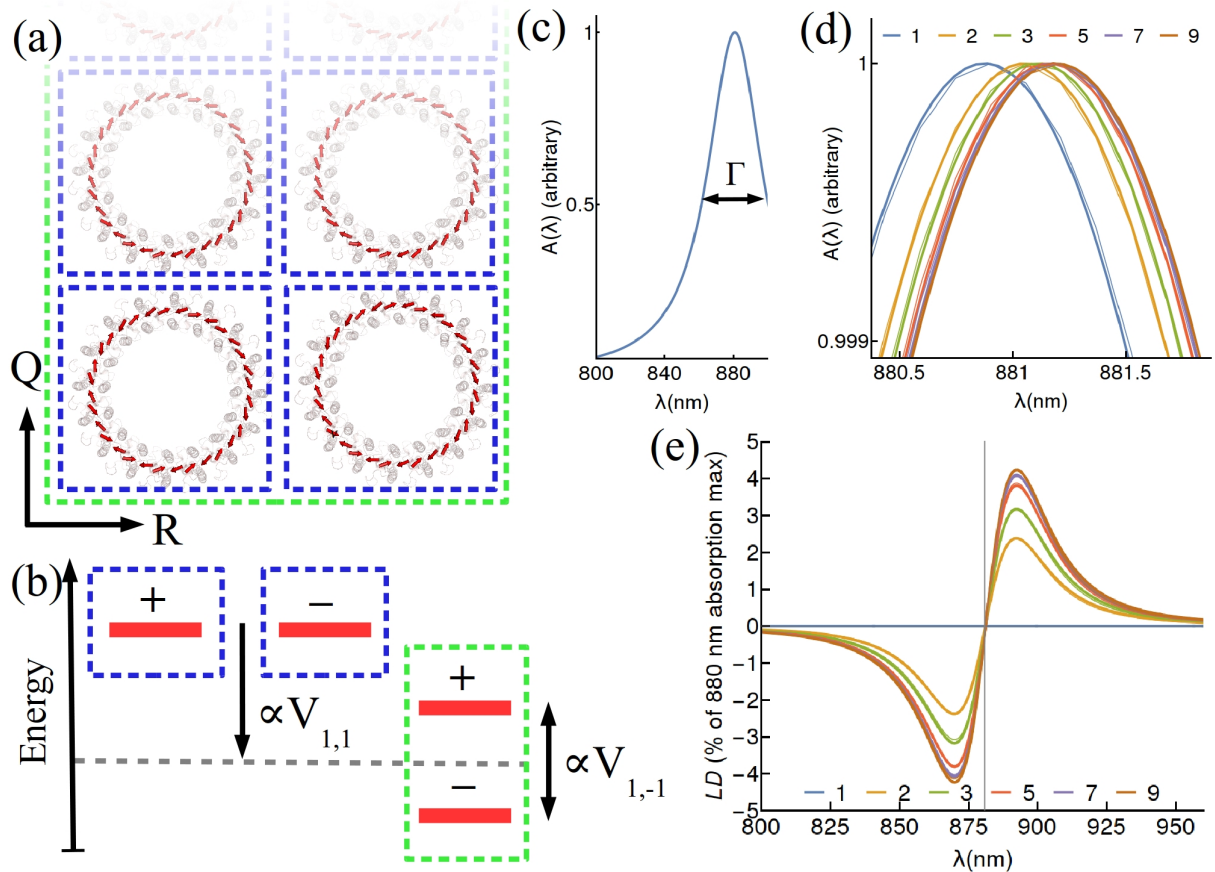


FIG. 3. (a) LH complexes in purple bacteria naturally arrange themselves in well-ordered 2D arrays. The spectral consequences of extended delocalization in such an arrangement can be understood by examining a rectangular $Q \times R$ array. The absorption anisotropy is strongest for linear-like arrays ($Q/R \gg 1$), represented schematically by the color gradient. (b) The circular symmetry of single LH complexes concentrates the optical absorption strength in degenerate states with orthogonal polarization (blue bounding boxes). The circular symmetry of the combined system is broken upon interaction (green bounding boxes), leading to a measurable splitting of polarized states. (c) Room temperature absorption spectra of LH1 shows a single peak around 880 nm of width Γ . (d) Red-shifted absorption and (e) non-zero linear-dichroism (LD) for linear arrays ($Q=1$, calculated for different values of $R = 1, \dots, 9$) witness extended delocalization over multiple LH1 complexes. Full numerical simulations (thin lines) are indistinguishable from homogeneous dressing procedure (thick lines).

figuration. The energies of these states are shifted by

$$\begin{aligned}
 E_{\pm} &= 2V_{1,1} \left(\cos\left(\frac{\pi}{Q+1}\right) + \cos\left(\frac{\pi}{R+1}\right) \right) \\
 &\pm 2V_{1,-1} \left(\cos\left(\frac{\pi}{Q+1}\right) - \cos\left(\frac{\pi}{R+1}\right) \right) \\
 &= \delta E \pm \Delta E.
 \end{aligned} \tag{6}$$

From the above expression a common red shift $\delta E = (E_+ + E_-)/2 \propto V_{1,1}$ arises for both bright transitions. Given that the absorption is composed of red-shifted states, a general red shift of the (unpolarised) absorption maximum, with respect to the single-ring case, is expected for the coherently coupled array of rings.

The states $|+\rangle$ and $|-\rangle$ are orthogonally polarized; polarisation along the \hat{x} -axis results in absorption spectra peaking at energy E_+ corresponding to $\vec{D}_+ \propto \hat{x}$, while polarisation along the \hat{y} -axis results in absorption spectra peaking at energy E_- corresponding to the $\vec{D}_- \propto \hat{y}$

state. The subtraction of these two spectra recorded from perpendicular polarisations, described by the LD of 3, is finite whenever $\Delta E = (E_+ - E_-)/2$ does not vanish, which occurs, according to 6, strictly due to the coherent coupling $V_{k,k'}$ which breaks the circular symmetry of the assembly. Explicitly, based on 6 the effect is greatest for a linear chain ($Q = 1$ or $R = 1$) and a saturation for both the red shift, δE , and splitting, ΔE , is expected, as $\cos \frac{\pi}{Q+1} \approx 1$ already for $Q \approx 7 - 8$ rings.

The key theoretical predictions of this article are summarized in Figures 3(d)-(e). Namely, a red shift in the unpolarised absorption spectra and a non-zero LD will be observable at room temperature due to the coherent interaction between LH complexes in arrays with a large aspect ratio and small width, i.e. linear-like arrays. As shown in the figure, full numerical simulations agree completely with a simple dressing of this analytic model with a Lorentzian lineshape with FWHM of Γ . Consequently,

the amplitude of the *LD*, which can be obtained from the Lorentzian lineshapes, is given by

$$LD_{max} = C_1 \frac{|V_{1,-1}|}{\Gamma} + O\left(\left(\frac{|V_{1,-1}|}{\Gamma}\right)^3\right) \quad (7)$$

where the constant $C_1 = \frac{3\sqrt{3}}{2}$ in the case of two rings, accounts for the geometrical details of the array. Note that an assembly of uncoupled rings is described by a statistical mixture of single-ring excitons, and hence shows zero *LD*. A non-zero *LD* signal quantifies the inter-ring coupling, as these spectral changes result strictly as a consequence of the extended delocalization which breaks the circular symmetry of single-ring excitons. Importantly, the saturation observed in long chains for both *LD* amplitude and red shift follows directly from 6, and follows as a consequence from longer arrays which present greater delocalization lengths. Further details from the excitonic delocalization length as the number of rings increase are presented in the Supplementary information.

Inhomogeneous broadening. The spectral lineshape and width are determined by both homogeneous and inhomogeneous contributions. Two effects are manifested when inhomogeneities are introduced in excitonic transitions, namely, lineshape modifications and energy shifts. Figures 4(a-c) show the effect of inhomogeneous broadening on the lineshape. The inhomogeneous linewidths are dressed with Lorentzian homogeneous lineshapes such that the FWHM of the full spectrum remains constant. The inhomogeneities produce an overall absorption lineshape with more Lorentzian (for low inhomogeneous disorder) or Gaussian (for high disorder) character, as can be observed in Fig.4(a). For all values of inhomogeneous disorder, bounded by the full spectral width, the energy splitting between absorption spectra along orthogonal polarizations remains constant, as presented in Figure 4(b). This analysis supports, thereby, a minor change in the *LD* with inhomogeneous disorder (see Figure 4(c)), arising solely from the Lorentzian or Gaussian character of the absorption lineshape.

Inter-complex perturbations. The inhomogeneous model presented above accounts for environmentally-induced inhomogeneities in the pigment energies and nearest-neighbour couplings. However, it does not account for explicit structural perturbations, such as variations in the inter-complex distance, discussed here, and elliptical perturbations, discussed below. Examination of paracrystalline⁴⁴ domains of LH2 in *Rsp. photometricum* and close-packed orthorhombic crystals^{45,46} in *R. rubrum* imply variations of only a few Angstroms in center-to-center distances^{44,47}. Figure 4(d) shows the effect on the *LD* when the inter-complex distance is varied by an amount much greater than the variations observed from pair correlation functions calculated from atomic force microscopy (AFM) experiments ($\sqrt{\langle \delta r^2 \rangle} = 0, 5, 10$ Å as compared to $\sqrt{\langle \delta r^2 \rangle} \sim 1$ Å⁴⁴). This figure illustrates that the contrast in the *LD* actually increases with greater center-to-center distance variations. This

surprising result can be understood from the functional form of the Coulomb interaction: the $1/r^3$ dependence means that bringing rings together by δr increases the coupling more than it is decreased by separating them by δr . Hence, the *LD* is enhanced in average. However, note that the few Angstrom variations observed in experiments are too small to appreciably affect the *LD* signal.

Elliptical perturbations. In general, LH complexes in purple bacteria express geometries which may differ from the circular ring of *R. rubrum* in our model. Another conformation of the LH1 in *R. rubrum* has been observed to be significantly ellipsoidal⁴⁸. In addition, the LH2 of *Rubrivax gelatinosus*, obtained by AFM⁴⁹, and the latest LH1 X-ray structure of *Tch. tepidum* both exhibit a degree of ellipticity³³. It is not known if the long axes of elliptical rings may be aligned or randomly oriented. A study of elliptical structures is therefore in order as it might clarify the scope of the *LD* to witness extended delocalization.

Oval structures with an apparently small eccentricity $\sqrt{1 - (\frac{a}{b})^2} = 0.32$, where a and b are the minor and major axes, respectively, produce energy shifts among $k = \pm 1$ states of $\simeq 100$ cm⁻¹ in a single ring⁵⁰, which is 5-10 times larger than the shifts due to inter-ring excitonic coupling. In these experiments the excitation polarisation was fixed with respect to the major axis of the single elliptical ring. In an ensemble, there is no reason to believe that the orientations of major axes will or not will correlate. If an ensemble presents randomly-oriented major axes and the rings do not couple coherently, then the finite *LD* signals, stemming from the elliptical geometries, cancel out and lead to a vanishing *LD* (see Fig. 4(e)). In the same fashion, if an ensemble of randomly-oriented coupled rings is considered, then the *LD* arising from the elliptical perturbation vanishes and only the nonzero signal arising from the coherent interaction remains. Figure 4(e) shows that the nonzero *LD* for coherently-coupled linear arrays is robust to the ensemble-averaged elliptical perturbation (compare with Fig. 3(e)), and hence remains a signature of excitonic delocalisation over the array. In addition, for structures that present a finite *LD* at the single-ring level, a *change* in the *LD* with the assembly size arises solely from the extended delocalization over the array of complexes (for further information about such a scenario, refer to the Supporting Information).

Experimental determination of Förster rates. Besides controlling the linear optical response, the coherent coupling dictates the rate at which, on a longer time scale, excitations migrate incoherently between complexes⁵³. The transfer among different bands which can be resolved spectrally permits experimental schemes that make use of the different spectral components in order to separate dynamical contributions⁵⁴⁻⁵⁸. In the case of isoenergetic transfer steps, like LH1→LH1, this is not possible and it becomes hard to identify the nature of individual dynamical components. Techniques based

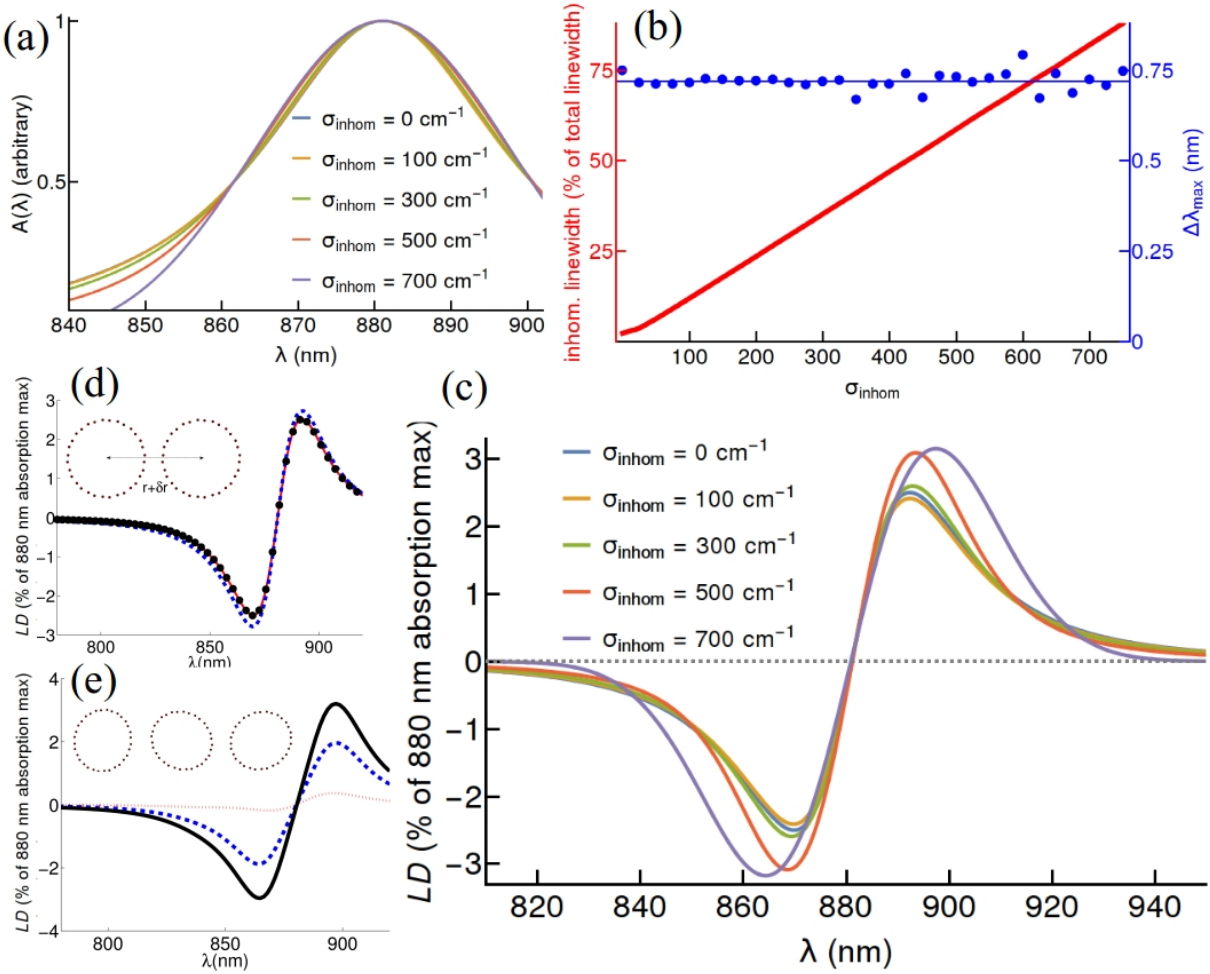


FIG. 4. Effects of energetic and structural disorder on LD. In (a), the overall lineshape takes on more Gaussian character as inhomogeneous disorder is increased. The levels of disorder considered here lead to inhomogeneous linewidths which are up to 75% of the overall linewidth, as illustrated in (b). The splitting between orthogonally-polarized manifolds, $\Delta\lambda_{max}$, in (b), remains constant. Consequently, the LD signal (c) is robust to energetic disorder ($\sigma_{inhom} = 0 - 700 \text{ cm}^{-1}$), bounded by the full spectral width. The LD is also robust to variations of the inter-ring distance, as shown in (d) ($\sqrt{\langle \delta r^2 \rangle} = 0, 5, 10 \text{ \AA}$ in solid, dots, and dashed, respectively). In (e) the LD ensemble averaged over randomly-oriented oval structures in linear arrays with 1, 2 and 3 rings (solid, dashed and dotted, respectively).

on transient depolarization, such as anisotropy absorption recovery, have been valuable to recognize multiple dynamical contributions at low temperatures in the core complex of *R. rubrum*⁵⁹⁻⁶⁵, but have failed to unequivocally identify components arising from intra-ring relaxation or from inter-ring energy transfer. The accurate determination of these rates is crucial for understanding the efficiency of photosynthesis.

We show here that the possibility to obtain the coherent coupling among isoenergetic species of LH1 or LH2 complexes—through the absorption measurements illustrated in Figure 3—circumvents the ambiguity in these isoenergetic landscapes and opens up a promising experimental scheme to quantify their mutual transfer rates. Generalized Förster theory is often used to calculate the rate of incoherent transfer $\gamma_{k \rightarrow k'}$ from a donor exciton k

to acceptor exciton k'

$$\gamma_{k \rightarrow k'} = \frac{2\pi}{\hbar} |V_{k,k'}|^2 Z_k I_{k,k'}, \quad (8)$$

where $V_{k,k'}$ is, as before, the coherent excitonic coupling among single-ring states, Z_k is the thermal population (Boltzmann factor) and $I_{k,k'} = \int_0^\infty F_k(\epsilon) A_{k'}(\epsilon) d\epsilon$ denotes the spectral overlap integral of the donor fluorescence from exciton k and acceptor absorption of exciton k' , F and A , respectively^{37,66}. The total transfer rate from donor to acceptor is $\gamma = \sum_{k,k'} \gamma_{k \rightarrow k'}$. We have shown that absorption at physiological temperatures is predominantly homogeneous, and under the assumption that the emission is also spectrally homogeneous, it is $\gamma \approx \sum_{k,k'=\pm 1} \gamma_{k \rightarrow k'}$, and the Förster rate can be calcu-

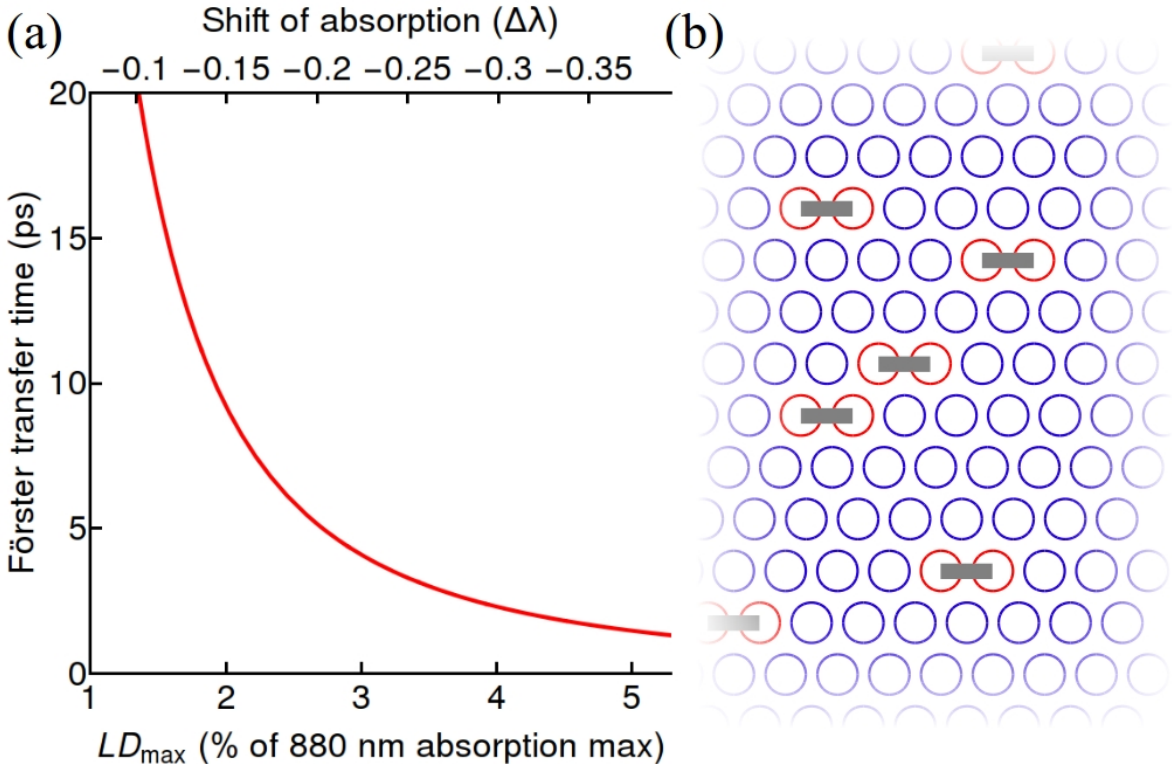


FIG. 5. Absorption measurements can provide direct information on the magnitude of transfer rates. In (a) is presented the transfer time between LH1 complexes as a function of the *LD* contrast and/or shift in the unpolarized absorption (which depend on the coherent coupling $V_{k,k'}$, itself a function of the dielectric constant). An experimental ensemble measurement of the *LD* signal mitigates the effects of structural disorder and allows a direct absorption readout. Such an experiment is shown in (b), where “blue” rings, mutated to maximally absorb at less than 880 nm^{51,52}, are grown in a membrane with “red” rings, absorbing at 880 nm and linked in pairs. The aggregation of blue-shifted LH1s leads to their vanishing *LD*, while, if the axes of the red pairs align, their non-zero *LD* signal can be measured.

lated as

$$\gamma = \frac{2\pi}{\hbar} (2|V_{1,1}|^2 + 2|V_{1,-1}|^2) Z_1 I \quad (9)$$

where $I = \int_0^\infty F(\epsilon)A(\epsilon)d\epsilon$ is the full spectral overlap and Z_1 is the thermal population of the $|k = \pm 1\rangle$ states, which depends on the single-ring model. As shown above, $V_{1,1}$ and $V_{1,-1}$ are quantified by shifts in absorption and non-zero *LD* contrast, respectively, a measurement of which allows a calculation of the Förster rate with a minimum of model input. Parameters able to reproduce absorption spectra²⁶ (see Supporting Information) predict an inter-ring transfer time of 4.75 ps, which is well within the bounds (~ 1 ps – 20ps) of current experiments and calculations^{32,60,65}. Determination of the inter-ring coupling strength by measurement of the *LD* thus provides a new method to determine Förster transfer rates. Moreover, this would then provide further insight into the values of the dielectric constant and the BChl dipole moment *in vivo*, which are parameters usually estimated indirectly. Figure 5 (a) plots the transfer time, *LD* contrast and absorption shift as a function of these quantities according to 9.

Several elements have to be brought together in an ex-

periment which confirms excitonic delocalization across extended domains. A speculative setup is illustrated in Figure 5 (b) based on mutagenesis of blue-shifted LH1s^{51,52}. If a link between LH1s by means of mechanical bridges or affinity domains is accomplished, the formation of linear-like assemblies will be possible. Additionally, these assemblies must be *macroscopically* aligned in order to set the polarisation excitation directions. The blue-shifted LH1s will serve then to build the membrane scaffold to accomodate the linear arrays of non-mutated LH1s and fix their orientations. Fluorescence yield detection upon polarised excitation performed on single assemblies³⁴ is also a promising technique to confirm/disregard the hypothesis of long-range excitonic delocalisation in natural LH aggregates.

IV. CONCLUSIONS

In summary, we have modeled and characterized, through analytical expressions and numerical calculations, the optical response due to coherent coupling between multiple rings in photosynthetic membranes of purple bacteria. This investigation highlights the im-

portance of a description, at room temperature, of light absorption beyond the standard assumption of excitons restricted to individual rings. The dipole moment redistribution that emerges in 2D arrays of LH1 rings, due to extended excitons, leads us to propose an experimental procedure, based on polarized and unpolarized absorption spectra of small linear-like arrays of rings, which quantifies inter-ring coherent coupling. We show that this experimental procedure allows an alternative, indirect measurement of their incoherent Förster transfer rate, which carries additional information on currently poorly-characterized parameters, like the dielectric constant or the *in vivo* BChls dipole moment. Such a measurement could be accomplished through absorption of an ensemble of oriented linear-like assemblies or through fluorescence yield detection of single assemblies which have been excited by polarized fields.

ACKNOWLEDGEMENTS

This work was funded by the EU STREP project PA-PETS, the ERC Synergy grant BioQ and an Alexander von Humboldt Professorship. Additional support was provided by the National Science Foundation through PFC@JQI and the National Science Foundation Graduate Research Fellowship Program under DGE-1322106. Any opinions, findings, and conclusions and recommendations expressed in this material are those of the authors and do not necessarily reflect the views of the National Science Foundation. The authors would like to thank R. Ghosh (University of Stuttgart), F. Jelezko (University of Ulm) and Shai Machnes (Weizmann Institute, Israel) for discussion at early stages of this work, and R. Ghosh for a careful and critical reading of the manuscript.

Supporting information includes a study of the effects of inhomogeneous broadening on measures of exciton delocalization and a generalization of the results to alternate membrane geometries.

¹R. W. Visschers, M. C. Chang, F. van Mourik, P. S. Parkes-Loach, B. A. Heller, P. A. Loach, and R. van Grondelle, "Fluorescence polarization and low-temperature absorption spectroscopy of a subunit form of light-harvesting complex i from purple photosynthetic bacteria," *Biochem.* **30**, 5734–5742 (1991).

²S. Karrasch, P. A. Bullough, and R. Ghosh, "The 8.5 Å projection map of the light harvesting complex I from *Rhodospirillum rubrum* reveals a ring composed of 16 subunits," *EMBO Journal* **14**, 631 (1995).

³S. Bahatyrova, R. N. Freese, C. A. Siebert, J. D. Olsen, K. A. van der Werf, R. van Grondelle, R. A. Niederman, O. A. Bullough, C. Otto, and N. C. Hunter, "The native architecture of a photosynthetic membrane," *Nature* **430**, 1058 (2004).

⁴S. Scheuring, R. P. Goncalves, V. Prima, and J. Sturgis, "The photosynthetic apparatus of *Rhodopseudomonas palustris*: Structure and organization," *Journal of Molecular Biology* **358**, 83 (2006).

⁵A. P. Shreve, J. K. Trautman, H. A. Franck, T. G. Owens, and A. C. Albrecht, "Femtosecond energy-transfer processes in the b800-b850 light-harvesting complex of rhodobacter sphaeroides 2.4.1," *Biochim. Biophys. Acta* **1058**, 280–288 (1991).

⁶C. A. Siebert, P. Qian, D. Fotiadis, A. Engel, N. C. Hunter, and P. A. Bullough, "Molecular architecture of photosynthetic membranes in *Rhodobacter sphaeroides*: the role of PufX," *EMBO Journal* **23**, 690 (2004).

⁷X. Hu, T. Ritz, A. Damjanović, F. Authennrieth, and K. Schulten, "Photosynthetic apparatus of purple bacteria," *Quarterly Review of Biophysics* **35**, 1–62 (2002).

⁸J. Strumpfer and K. Schulten, "Excited state dynamics in photosynthetic reaction center and light harvesting complex 1," *J. Chem. Phys.* **137**, 065101 (2012).

⁹R. C. Cheng and R. J. Silbey, "Coherence in the b800 ring of purple bacteria lh2," *Phys. Rev. Lett.* **96**, 028103–028106 (2006).

¹⁰J. Strümpfer, M. Séner, and K. Schulten, "How quantum coherence assists photosynthetic light-harvesting," *J. Phys. Chem. Lett.* **3**, 536–542 (2012).

¹¹E. Romero, R. Augulis, V. I. Novoderezhkin, M. Ferreti, J. Thieme, E. Zigmantas, and R. van Grondelle, "Quantum coherence in photosynthesis for efficient solar-energy conversion," *Nature Phys.* **10**, 676–682 (2014).

¹²F. Fuller, J. Pan, A. Gelzinis, V. Butkus, S. Seckin Senlik, D. E. Wilcox, C. Yocom, L. Valkunas, D. Abramavicius, and J. P. Ogilvie, "Vibronic coherence in oxygenic photosynthesis," *Nature Chem.* **6**, 706–711 (2014).

¹³H. Lee, Y. C. Cheng, and G. R. Flemming, "Coherence dynamics in photosynthesis: Protein protection of excitonic coherence," *Science* **316**, 1462–1465 (2007).

¹⁴G. Panitchayangkoon, K. A. Hayes D., Fransteda, E. Caram J. R., Harel, J. Wen, R. Blankenship, and G. S. Engel, "Long-lived quantum coherence in photosynthetic complexes at physiological temperature," *PNAS* **107**, 12766–12770 (2010).

¹⁵G. Engel, T. Calhoun, E. Read, T. Ahn, T. Mancal, Y. Cheng, R. Blankenship, and G. Fleming, "Evidence for wavelike energy transfer through quantum coherence in photosynthetic systems," *Nature* **446**, 782–786 (2007).

¹⁶T. Brixner, J. Stenger, H. M. Vaswani, M. Cho, R. E. Blankenship, and R. G. Fleming, "Two-dimensional spectroscopy of electronic couplings in photosynthesis," *Nature* **434**, 625–628 (2005).

¹⁷D. Hayes, G. Panitchayangkoon, K. A. Fransted, J. R. Caram, J. Wen, K. F. Freed, and G. S. Engel, "Dynamics of electronic dephasing in the Fenna-Matthews-Olson complex," *New J. Phys.* **12**, 065042 (2010).

¹⁸M. Mohseni, P. Rebentrost, S. Lloyd, and A. Aspuru-Guzik, "Environment-assisted quantum walks in photosynthetic energy transfer," *J. Chem. Phys.* **129**, 174106 (2008).

¹⁹M. B. Plenio and S. F. Huelga, "Dephasing-assisted transport: Quantum networks and biomolecules," *New J. Phys.* **10** (2008).

²⁰A. Olaya-Castro, C. Lee, F. Olsen, and N. Johnson, "Efficiency of energy transfer in a light-harvesting system under quantum coherence," *Phys. Rev. B* **78**, 085115 (2008).

²¹F. Autenrieth, *The photosynthetic apparatus of Rhodospirillum rubrum: a computational approach*, Diploma thesis, University of Stuttgart (2002).

²²J. Adolphs and T. Renger, "How proteins trigger excitation energy transfer in the fmo complex of green sulfur bacteria," *Bioophys. J.* **91**, 2778–2797 (2006).

²³J. Strumpfer and K. Schulten, "Light harvesting complex ii b850 excitation dynamics," *J. Chem. Phys.* **131**, 225101 (2009).

²⁴K. Timpmann, G. Trinkunas, P. Qian, C. Hunter, and A. Freiberg, "Excitons in core LH1 antenna complexes of photosynthetic bacteria: Evidence for strong resonant coupling and off-diagonal disorder," *Chemical Physics Letters* **414**, 359–363 (2005).

²⁵G. Trinkunas and A. Freiberg, "A disordered polaron model for polarized fluorescence excitation spectra of lh1 and lh2 bacteriochlorophyll antenna aggregates," *Journal of Luminescence* **119–120**, 105–110 (2006).

²⁶F. Caycedo-Soler, C. A. Schroeder, C. Autenrieth, R. Ghosh, S. F. Huelga, and M. B. Plenio, "Quantum delocalization directs antenna absorption to photosynthetic reaction centres," *submitted* (2015).

²⁷X. Hu, T. Ritz, A. Damjanovic, A. Autenrieth, and K. Schulten, "Photosynthetic apparatus of purple bacteria." *Quart. Rev. of Biophys.* **35**, 1–62 (2002).

²⁸S. Scheuring, J. Busselez, and D. Levy, "Structure of the dimeric PufX-containing core complex of *Rhodobacter sphaeroides*," *Journal of Biological Chemistry* **279**, 3620 (2005).

²⁹S. Scheuring, J. N. Sturgis, V. Prima, D. Bernadac, Levi, and J. L. Rigaud, "Watching the photosynthetic apparatus in native membranes," *Proceeding of National Academy of Sciences USA* **101**, 1193 (2004).

³⁰T. Walz and R. Ghosh, "Two-dimensional crystallization of the light-harvesting I-reaction centre photounit from *Rhodospirillum rubrum*," *J. Mol. Biol.* **265**, 107–111 (1997).

³¹F. Caycedo-Soler, F. J. Rodríguez, L. Quiroga, and N. F. Johnson, "Light-Harvesting mechanism of bacteria exploits a critical interplay between the dynamics of transport and trapping," *Phys. Rev. Lett.* **104**, 15832 (2010).

³²T. Ritz, S. Park, and K. Schulten, "Kinetics of excitation migration and trapping in the photosynthetic unit of purple bacteria," *J. Phys. Chem. B* **105**, 8259–8267 (2001).

³³S. Satomi Niwa, L. J. Yu, K. Takeda, Y. Hirano, T. Kawakami, Z. Y. Wang-Otomo, and T. Miki, .

³⁴U. Gerken, D. Lupo, C. Tietz, J. Wrachtrup, and R. Ghosh, "Circular symmetry of the light-harvesting 1 complex from *rhodospirillum rubrum* is not perturbed by interaction with the reaction center," *Biochemistry* **42**, 10354–10360 (2003).

³⁵H. van Amerongen, L. Valkunas, and R. van Grondelle, *Photosynthetic excitons* (World Scientific Publishing Co. Pte. Ltd., 2000).

³⁶R. Monshouwer, M. Abrahamsson, F. van Mourik, and R. van Grondelle, "Superradiance and exciton delocalization in bacterial photosynthetic light-harvesting systems," *J. Phys. Chem. B* **101**, 7241–7248 (1997).

³⁷G. D. Scholes, "Long-range resonance energy transfer in molecular systems," *Ann. Rev. Phys. Chem.* **54**, 57–87 (2003).

³⁸A. Freiberg and K. Timpmann, "Picosecond fluorescence spectroscopy of light-harvesting antenna complexes from *Rhodospirillum rubrum* in the 300–4 K temperature range. Comparison with the data on chromatophores," *J. Photochem. Photobiol B; Biol.* **15**, 151–158 (1992).

³⁹H. Kramer, J. Pennoyer, R. van Grondelle, W. Westerhuis, R. Niedermann, and J. Amesz, "Low-temperature optical properties and pigment organization of the B875 light-harvesting bacteriochlorophyll-protein complex of purple photosynthetic bacteria," *Biochim. Biophys. Acta* **767**, 335–344 (1984).

⁴⁰C. Rijgersberg, R. van Grondelle, and J. Amesz, "Energy transfer and bacteriochlorophyll fluorescence in purple bacteria at low temperature," *Biochim. Biophys. Acta* **592**, 53–64 (1980).

⁴¹D. J. Thouless, "Electrons in disordered systems and the theory of localization," *Phys. Rep.* **13**, 93–142 (1974).

⁴²A. Davydov, "The theory of molecular excitons," *Usp. Fiz. Nauk* **82**, 393–448 (1964).

⁴³H.-M. Wu, M. Ratsep, I.-J. Lee, R. Cogdell, and G. Small, "Exciton level structure and energy disorder of the B850 ring of the LH2 antenna complex," *J. Phys. Chem. B* **101**, 7654–7663 (1997).

⁴⁴S. Scheuring and J. Sturgis, "Chromatic adaptation of purple bacteria," *Science* **309**, 484 (2005).

⁴⁵R. Ghosh, J. Kessi, H. Hause, E. Wherli, and R. Bachofen, *Molecular biology of membrane-bound complexes in phototrophic bacteria*, edited by G. Drews and E. A. Dawes (Plenum Press, New York, 1990) pp. 245–251.

⁴⁶S. J. Jamieson, P. Wang, P. Qian, J. Y. Kirkland, M. J. Conroy, C. N. Hunter, and P. Bullough, "Projection structure of the photosynthetic reaction centre-antenna complex of *Rhodospirillum rubrum* at 8.5 Å resolution," *EMBO J.* **21**, 3927–3935 (2002).

⁴⁷S. Scheuring, J. L. Rigaud, and J. N. Sturgis, "Variable LH2 stoichiometry and core clustering in native membranes of *Rhodospirillum photometricum*," *EMBO* **23**, 4127 (2004).

⁴⁸S. J. Jamieson, P. Wang, P. Qian, J. Y. Kirkland, M. J. Conroy, C. N. Hunter, and P. Bullough, "Projection structure of the photosynthetic reaction centre-antenna complex of *Rhodospirillum rubrum* at 8.5 Å resolution," *EMBO J.* **21**, 3927–3935 (2002).

⁴⁹S. Scheuring, F. Reiss-Husson, A. Engel, J.-L. Rigaud, and J.-L. Ranck, "High-resolution AFM topography of *Rubrivax gelatinosus* light-harvesting complex LH2," *EMBO J.* **20**, 3029–3035 (2001).

⁵⁰U. Gerken, F. Jelezko, B. Götze, M. Branschädel, C. Tietz, R. Ghosh, and J. Wrachtrup, "Membrane environment reduces the accessible conformational space available to an integral membrane protein," *J. Phys. Chem. B* **107**, 338–343 (2003).

⁵¹R. Ghosh, H. Hauser, and R. Bachofen, "Reversible dissociation of the B873 light-harvesting complex from *Rhodospirillum rubrum* G9+," *Biochemistry* **27**, 1004–1014 (1988).

⁵²J. D. Olsen, J. Sturgis, W. H. J. Westerhuis, G. J. S. Fowler, C. N. Hunter, and B. Robert, "Site-directed modifications of the ligands to the bacteriochlorophylls of the light-harvesting LH1 and LH2 complexes of *Rhodobacter sphaeroides*," *Biochemistry* **36**, 12625–12632 (1997).

⁵³T. Förster, *Delocalized excitation and excitation transfer*, edited by M.-M. Beyerle (Academic Press, New York, 1965) pp. 93–137.

⁵⁴A. Fidler, V. Singh, P. Long, P. Dahlberg, and G. Engel, "Probing energy transfer events in the light-harvesting complex 2 (LH2) of *Rhodobacter sphaeroides* with two-dimensional spectroscopy," *J. Chem. Phys.* **139**, 155101 (2013).

⁵⁵P. Dahlberg, A. Fidler, J. Caram, P. Long, , and G. Engel, "Energy transfer observed in live cells using two-dimensional electronic spectroscopy," *J. Phys. Chem. Lett.* **4**, 3636–3640 (2013).

⁵⁶B. Brüggermann, N. Christensson, and T. Pullerits, "Temperature dependent exciton-exciton annihilation in the LH2 antenna complex," *Chem. Phys.* **357**, 140–143 (2009).

⁵⁷S. Hess, M. Cachisvilis, K. E. Timpmann, M. Jones, G. Fowler, N. C. Hunter, and V. Sundstrom, "Temporally and spectrally resolved subpicosecond energy transfer within the peripheral antenna complex (lh2) and from lh2 to the core antenna complex in photosynthetic purple bacteria," *Proceedings National Academy of Sciences* **92**, 12333 (1995).

⁵⁸R. Hildner, D. Brinks, J. B. Nieder, R. J. Cogdell, and N. F. Van Hulst, "Quantum coherent energy transfer over varying pathways in single light-harvesting complexes," *Science* **340**, 1448–1451 (2013).

⁵⁹N. Hunter, H. Bergström, R. van Grondelle, and V. Sundström, "Energy-transfer dynamics in three light-harvesting mutants of *Rhodobacter sphaeroides*: a picosecond spectroscopy study," *Biochem.* **29**, 3202–3207 (1990).

⁶⁰V. Sundström, R. van Grondelle, H. Bergström, E. Åkesson, and T. Gillbro, "Excitation-energy transport in the bacteriochlorophyll antenna systems of *Rhodospirillum rubrum* and *Rhodobacter sphaeroides*, studied by low-intensity picosecond absorption spectroscopy," *Biochim. Biophys. Acta* **851**, 431–446 (1986).

⁶¹H. Bergström, W. Westerhuis, V. Sundström, R. van Grondelle, R. Niederman, and T. Gillbro, "Energy transfer within the isolated B875 light-harvesting pigment-protein complex of *Rhodobacter sphaeroides* at 77 K studied by picosecond absorption spectroscopy," *FEBS Lett.* **233**, 12–16 (1988).

⁶²T. Pullerits, K. Visscher, S. Hess, V. Sundström, A. Freiberg, K. Timpmann, and R. van Grondelle, "Energy transfer in the inhomogeneously broadened core antenna of purple bacteria: A simultaneous fit of low-intensity picosecond absorption and fluorescence kinetics," *Biophys. J.* **66**, 236–248 (1994).

⁶³S. Bradforth, R. Jimenez, F. van Mourik, R. van Grondelle, , and G. Fleming, "Excitation transfer in the core light-harvesting complex (LH-1) of *Rhodobacter sphaeroides*: an ultrafast fluorescence depolarization and annihilation study," *J. Phys. Chem.* **99**, 16179–16191 (1995).

⁶⁴H. Bergström, V. Sundström, R. van Grondelle, T. Gillbro, and R. Cogdell, "Energy transfer dynamics of isolated B800–B850 and B800–B820 pigment-protein complexes of *Rhodobacter sphaeroides* and *Rhodopseudomonas acidophila*," *Biochim. Biophys. Acta* **936**, 90–98 (1988).

⁶⁵V. Sundström and R. van Grondelle, "Kinetics of excitation

transfer and trapping in purple bacteria,” in *Anoxygenic photosynthetic bacteria* (Springer, 1995) pp. 349–372.

⁶⁶S. Jang, M. Newton, and R. Silbey, “Multichromophoric Förster resonance energy transfer,” *Phys. Rev. Lett.* **92**, 218301 (2004).

Appendix A: Measures of extended delocalization

Excitonic properties from purple bacteria membranes can be obtained from the Coulomb exchange Hamiltonian

$$H = \sum_m^{2NR} (\epsilon_m + \delta_{\epsilon_m}) |m\rangle \langle m| + \sum_{m \neq n}^{2NR} (J_{mn} + \delta_{J_{nm}}) (|n\rangle \langle m| + |m\rangle \langle n|) \quad (\text{A1})$$

where J_{nm} denotes the interaction strength between the induced transition-dipoles of pigments n and m , corresponding to electronic excited states $|n\rangle$ and $|m\rangle$ with energies ϵ_n and ϵ_m . Note that each ring contains $2N = 32$ pigments and we examine a line of rings ($Q=1$), as in the main text. The wavefunctions take a remarkable simple form in the absence of protein inhomogeneities ($\delta_{J_{nm}} = \delta_{\epsilon_m} = 0$), as given in eq (5) of the main text.

Explicitly, the bright states of relevance for the optical response are

$$|\pm, k_x = k_y = 1, Q = 1\rangle \propto \sum_r \sin\left(\frac{\pi}{R+1}\right) |\pm, r\rangle. \quad (\text{A2})$$

These states present populations in each ring proportional to $\sin^2(\pi r/(R+1))$ which is largest for the rings lying in the middle of the linear chain. Note that in the absence of coherent interaction among rings, all states should have populations concentrated in single rings. As a consequence, on average, a density operator will present a statistical mixture with populations being equally shared among all rings.

Absorption is a linear functional in the density operator. Hence, we concentrate on the density operator $\rho = |\alpha\rangle \langle \alpha|$ which results from averaging the eigenstates of eq (A1) under realistic conditions, i.e. with appropriate magnitude for protein induced fluctuations $\{\delta_\epsilon, \delta_J\} = \{60, 80\} \text{ cm}^{-1}$. Because the decoherence time is much longer ($\approx 100\text{-}200$ fs) than the absorption timescale (≈ 10 fs), we only consider quasi-static inhomogeneities for the description of the average density operator. Our choice of magnitude of these fluctuations is justified by a detailed analysis of absorption spectra of LH1 in *R. rubrum*, previously developed²⁶.

The average population of each ring for the subset of states $|\alpha\rangle$ with the largest light-induced dipole strength, is presented in Figure 6. Here, a non-uniform population in the linear configuration of rings can be seen, where the complexes in the middle of the chain present a greater population compared to the rings at the chain edges. The pattern of ring populations displayed in the presence of inhomogeneities resembles the noiseless case from states $|\pm, k_x = k_y = 1, Q = 1\rangle$, which illustrates the formation of excitons fulfilling the full array boundary conditions in the presence of quasi-static fluctuations.

The resilience of the excitons to the inhomogeneous disorder illustrates that the disorder is perturbative in a description of the full array properties. Another indicator of excitonic coherence among neighbouring rings is also presented in Figure 6, namely the total coherence $\rho_{r_1, r_2} = \sum_{n \in r_1, m \in r_2} |\langle n | \rho | m \rangle|$ among all chromophores that belong to neighbouring rings r_1 and r_2 . This total inter-ring coherence, usually assumed to be negligible for inter-ring exciton transfer, is manifestly non-zero in Figure 6, and is the cause for the absorption anisotropy that produces the finite linear dichroism (LD) discussed in the main text.

To characterise the excitons formed upon photon absorption, useful quantities are the conventional inverse participation ratio

$$IPR_C \equiv \left(\sum_i^{2NR} |c_i^\alpha|^4 \right)^{-1} \quad (\text{A3})$$

and a generalisation which we denote the ring inverse participation ratio

$$IPR_R \equiv \left(\sum_{r=1}^R \left(\sum_{i \in r}^N |c_i^\alpha|^2 \right)^2 \right)^{-1} \quad (\text{A4})$$

where the inner and outer sums are performed over BChls that belong to a specific ring r and over all rings in the array, respectively.

As defined, IPR_C ranges from 1 to the total number of pigments in the array and measures how many chromophores participate in a given exciton, while IPR_R ranges from 1 for any exciton confined to a single ring, to $IPR_R = R$ for pure states that are evenly delocalised over the entire array of R rings. For $IPR_R > 1$ or $IPR_C > 32$, these two quantities demonstrate unambiguously the presence of bright excitons over domains greater than a single ring (see Figure 7(a)). A general trend shows larger exciton lengths for arrays with higher number of rings. Figure 7(a) highlights realisations extending over more than 3 rings ($IPR_R > 3$), which extend well beyond the current paradigm of single ring excitons (lying flat with $IPR_R = 1$), sufficient for the description of processes occurring on a longer timescale.

The dependence of excitons length with the size of the array is made conspicuous in Figure 7(b) where the average \bar{IPR}_R is shown as a function of the linear ($Q = 1$) array size for the brightest state $|\alpha\rangle$ of each realisation. Here, it can be appreciated an increase in exciton size with the array extension in the same qualitative manner as the homogeneous wavefunctions of eq (A2) (also shown in the same figure).

Based on the observations that the wavefunction and the excitonic length from averages of inhomogeneous noise resemble qualitatively the features that arise from a noiseless treatment, it can be safely assumed that the inhomogeneous broadening is perturbative at room-temperature. It becomes natural therefore, to assert the

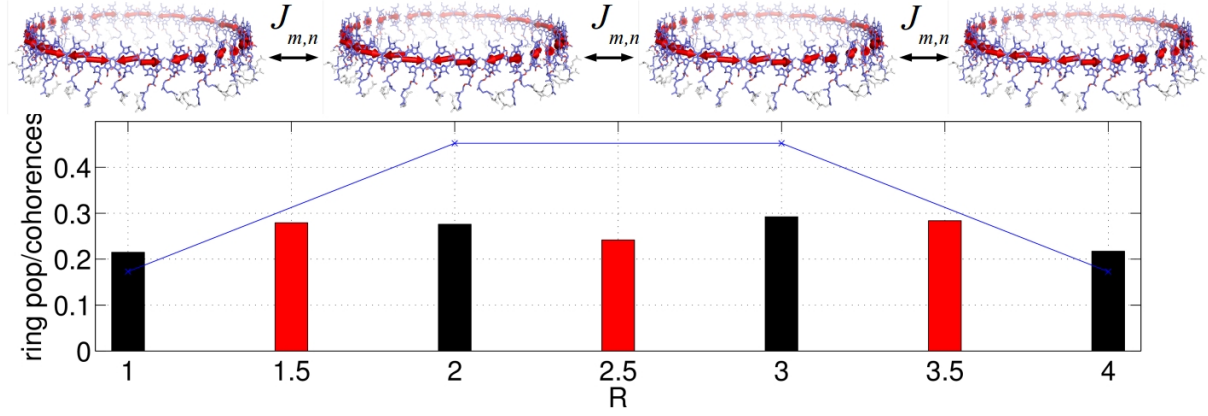


FIG. 6. The linear array of rings in top presents ring populations $\sum_{n_{er}} |\langle n | \rho | n \rangle|$ and total inter-ring coherences $\sum_{n_{er1}, n_{er2}} |\langle n_1 | \rho | n_2 \rangle| / 5$ (scaled down to fit the populations range) shown in black and red bars, as a result from averages of 5000 stochastic realisations of inhomogeneous noise. The result of the noise-less model for populations is presented in blue connected crosses.

properties of the system based on the noiseless characterization presented through equations (5)-(7) in the main text.

Appendix B: General 2D geometries

The description in the main text of excitonic delocalisation over extended domains made use of square unit-cell lattices. It was concluded that arrays with a large aspect ratio and small width are desirable in order to obtain an polarized optical response which encodes the symmetries of the extended excitons. Here we generalise these statements to arrays with other unit cells. Specifically, we analyse a triangular lattice and, to prove the generality of our statements, we also study a square unit cell with non-nearest-neighbour interactions.

The possibility to use the natural assembly of these complexes to probe inter-ring excitonic delocalization is investigated by numerical diagonalization of the Hamiltonian in the manifold $|k|, |k'| = 1$ for a triangular unit-cell lattice (Figure 8). The triangular unit cell approximates the natural “quasi-hexagonal” aggregation state observed for LH1 complexes in photosynthetic membranes of *R. rubrum*². Triangular para-crystalline domains of LH2 complexes also form in *Rsp. photometricum* at low light intensity conditions⁴. Figure 8(a), shows that the dipole strength in the triangular lattice is concentrated at the band edges, analogous to the prediction made by eqs (3-5) in the main text. As shown in this figure, states polarized along and perpendicular to the long-axis of the array are split in energy, leading to a finite *LD* once the stick spectra is dressed with appropriate line-shape functions. Figure 8(b) highlights another important feature. Here, even though an asymmetric array is being considered with the same aspect ratio, the *LD* signal is, in fact, smaller ($LD_{max} \approx 0.6\%$ in (b) as opposed to $LD_{max} \approx 0.75\%$ in (a)). This can be understood from eq (7) in the

main text, which shows that the energy splitting between bright states decreases for arrays of the same aspect ratio but increasing size. Hence, independent of unit-cell configurations, only arrays with a width of a few rings will be suitable to probe extended excitonic delocalization through *LD*.

The same conclusion can be drawn based on a square unit-cell with non-diagonal interactions, as shown in Figure 9. The additional interactions produce additional splittings, and arrays with appreciable aspect ratio ($Q/R \gg 1$ or $Q/R \ll 1$) still present a dipole moment redistribution that leads to polarization anisotropy. If the array is symmetric, the polarized states are not split in energy and the array shows zero *LD*, which can be seen from eq (7) in the main text. These results show that, independent of the unit-cell geometry, it is possible to witness *LD* in general arrays of small width and appreciable aspect ratio.

Appendix C: Hamiltonian of LH1 complex

In this study we have employed a model of the *R. rubrum* LH1 where 32 BChl molecules, bound to 16 α and β polypeptides as $\alpha\beta(\text{BChl})_2$ subunits, are arranged on two concentric α and β rings with C_{16} symmetry²⁶. The dipole-dipole interaction:

$$J_{n,m} = \frac{1}{4\pi\kappa} \left(\frac{\vec{d}_m \cdot \vec{d}_n}{|\Delta\vec{r}_{n,m}|^3} - \frac{3(\vec{d}_n \cdot \Delta\vec{r}_{n,m})(\vec{d}_m \cdot \Delta\vec{r}_{n,m})}{|\Delta\vec{r}_{n,m}|^5} \right), \quad (\text{C1})$$

where $\Delta\vec{r}_{n,m} = \vec{r}_n - \vec{r}_m$ and κ is the relative permittivity. The sub-nanometer distance between neighbouring chromophores implies that the nearest-neighbour couplings depend on the geometry of the electronic wavefunction of each chromophore and cannot be inferred

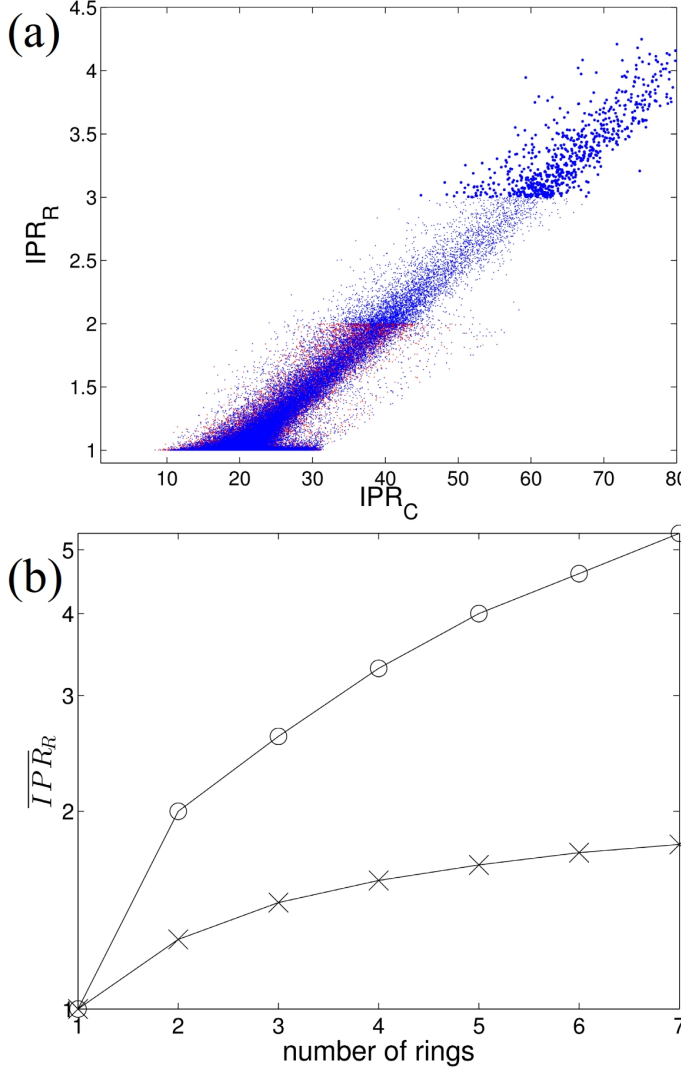


FIG. 7. (a) Scatter plot (points) of the IPR_C and IPR_R from eqs.(A3,A4) for two (red) and seven (blue) rings, for states with the greatest dipole moment in realisations of the quasi-static fluctuations in eq A1. States that delocalize beyond 3 rings are highlighted. In (b) is presented the average $\overline{IPR_R}$ for the brightest state in each noise realisation (crosses) and for the noiseless wavefunction in eq (A2) (circles), as a function of the length of the array. Symbols connected by straight lines to guide the eye.

directly from a dipolar interaction in the point dipole approximation. These couplings can be fitted using fluorescence anisotropy measurements, resulting in $Q_1 = 600 \text{ cm}^{-1}$ and $Q_2 = 377 \text{ cm}^{-1}$ for the intra- and inter-dimer couplings, respectively²⁴. The parameters required for the full numerical simulations are listed in Table 1.

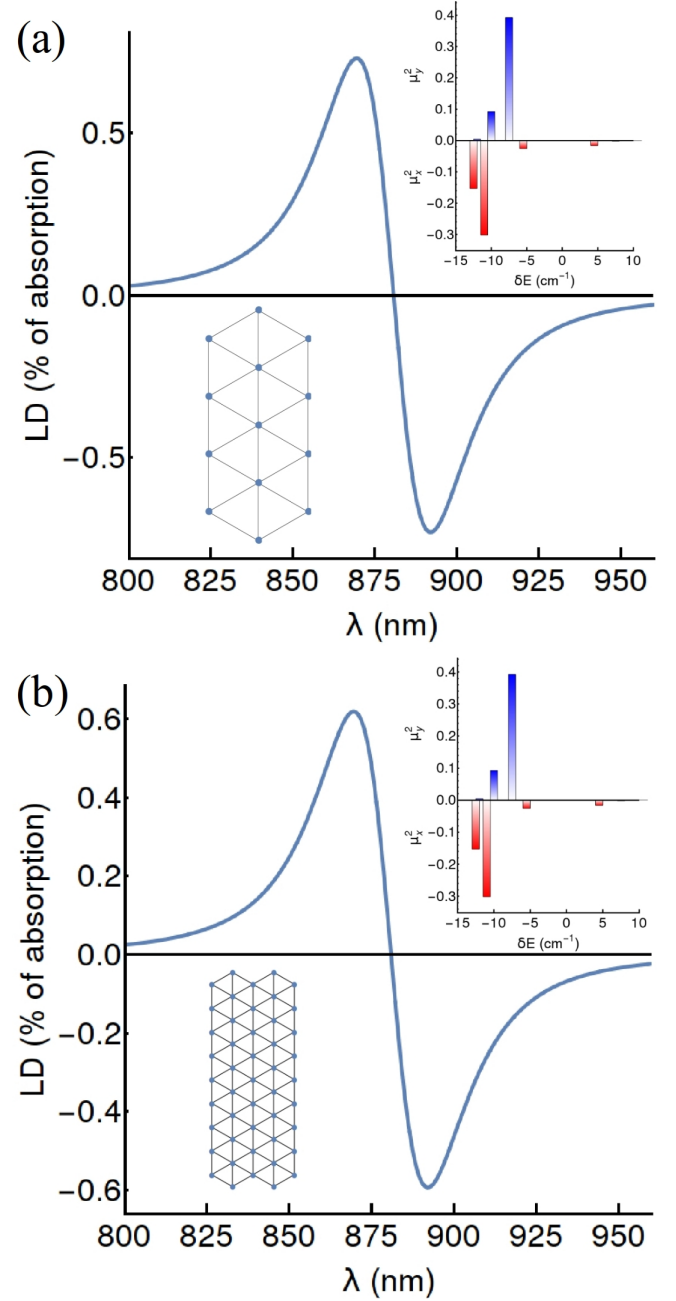


FIG. 8. LD spectra for the triangular lattice configuration and increasing array size. Insets show the lattice configuration studied and stick polarized spectra. A small asymmetric array, as in (a), exhibits a larger LD than its double (b) due to a decreased splitting of polarized states. This can be qualitatively understood from the results for the square unit-cell, eq (7) of the main text.

Appendix D: Procedure for species with finite linear dichroism from single ring complexes

The symmetry of a circular leads to a vanishing LD for isolated LH structures. However, different geometrical perturbations can indeed induce a finite linear dichroism

TABLE I. Parameters for the LH1 of *R. rubrum* used for numerical simulations²⁶

Parameter	Value	Description
γ	10.06°	intra-dimer angle
$\Delta\gamma_1, \Delta\gamma_2$	19.9°, 17.6°	dipole tilt away from tangent
ϕ_1, ϕ_2	6.24°, 4.81°	dipole tilt out of membrane plane
r_α, r_β	46.51 Å, 47.27 Å	radius of α, β rings
z	0.63 Å	vertical displacement among α and β chromophores
d	9.8 D	dipole moment for Q_y transition
κ	2	relative permittivity
$\epsilon_\alpha, \epsilon_\beta$	12646, 12656 cm ⁻¹	chromophore energies of α and β site
Q_1, Q_2	600, 377 cm ⁻¹	intra- and inter-dimer coupling
σ_J	60 cm ⁻¹	magnitude of nearest-neighbour coupling-strength disorder
σ	80 cm ⁻¹	magnitude energy disorder
G	465 cm ⁻¹	full-width half-maximum homogeneous dressing

at the level of single complexes and therefore, lead to an ambiguous estimation of excitonic delocalisation in the mentioned linear-like geometries. In order to investigate how to trace back the effects of extended excitonic delocalisation in the polarised optical response, we study a case of relevance, namely, elliptical structures as observed in *Tch. Tepidum* and cryo-electron microscopy in *R. rubrum*^{33,48}. In an ensemble of elliptical structures with randomly oriented major axes, it has been illustrated in Figure 4(e) in the main text, that the *LD* induced by such geometrical deformations averages to zero. However, it was observed that the macromolecular assembly in purple bacteria vesicles can indeed present long-range organisation⁷. Therefore, the likelihood of having affinity domains in each ring that set specific connecting residues to neighbouring units and result in an overall specific orientation of all major axes, is not out of question.

The scenario is presented in Figure 10 for a linear-like assembly where all major axes align. In such a case the *LD* signal is made *both* from single ring contributions and those arising from the extended delocalisation in the assembly. To recover a signal which does only present a *LD* from excitonic delocalisation, it suffices to subtract the contribution to the signal from individual rings, accomplished in principle, by the observation of the *LD* in isolated/individual rings.

The procedure is illustrated in Figure 10(b)-(c) where the *LD* for a single ring and for a linear-like assembly of

aligned elliptical LH1 complexes is presented. Since the major axis was chosen such that it produces a *LD* with opposite sign than that resulting from multiple ring excitonic delocalisation, the *LD* in (b) shows an amplitude that decreases with the number of coherently coupled rings. Nevertheless, the subtraction among any assembly and the signal from a single ring in (c), is able to assess the change in the optical response due the extended delocalisation as a function of the array size.

In general, if the geometrical contribution to the *LD* is independent of the size of the assembly, then a simple subtraction among *LD* signals, ΔLD , arising from different assemblies lengths will therefore represent the residual contribution resulting from the extended excitonic delocalisation among such assemblies.

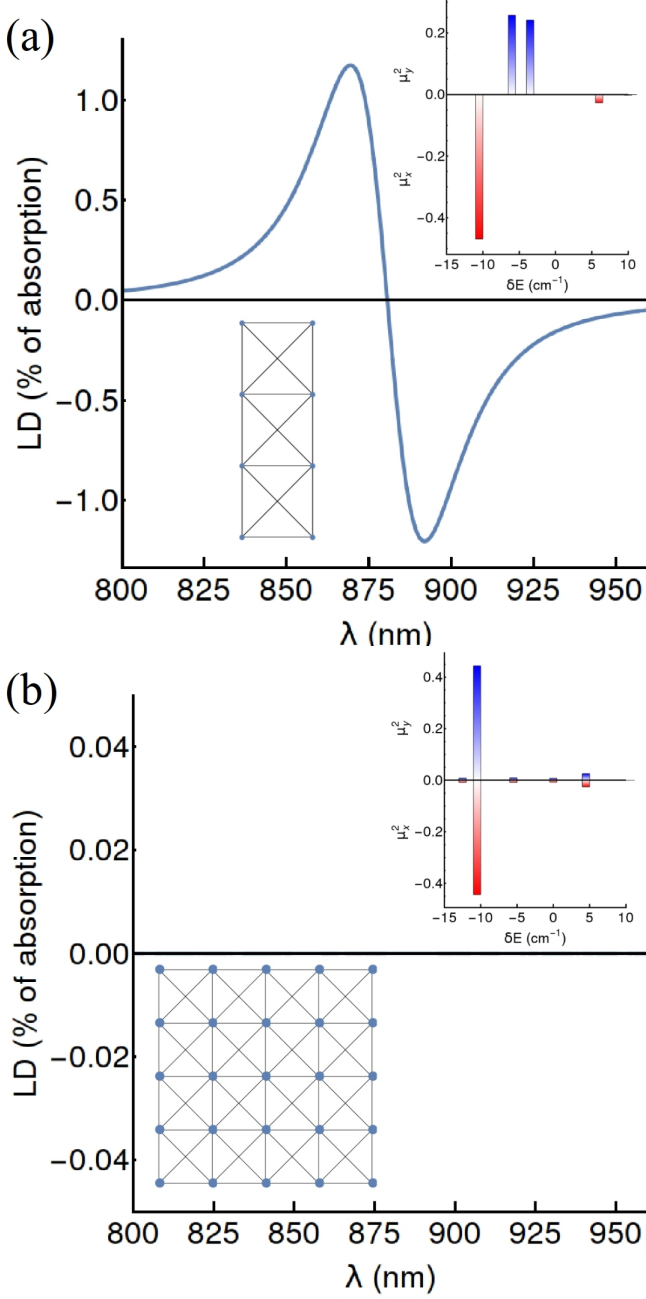


FIG. 9. *LD* spectra for the square lattice configuration and non-nearest-neighbor interactions. Insets show the lattice configuration studied and stick polarized spectra. The strip of dimers in (a) reflects the native organization of LH1s in membranes containing LH1 and LH2, and exhibits a non-zero *LD*. Symmetric arrays ($Q = R$), as in (b), show zero *LD* since the polarized states are degenerate in energy. These results are qualitatively similar to those for the square unit-cell with nearest-neighbor interactions, eq (7) of the main text.

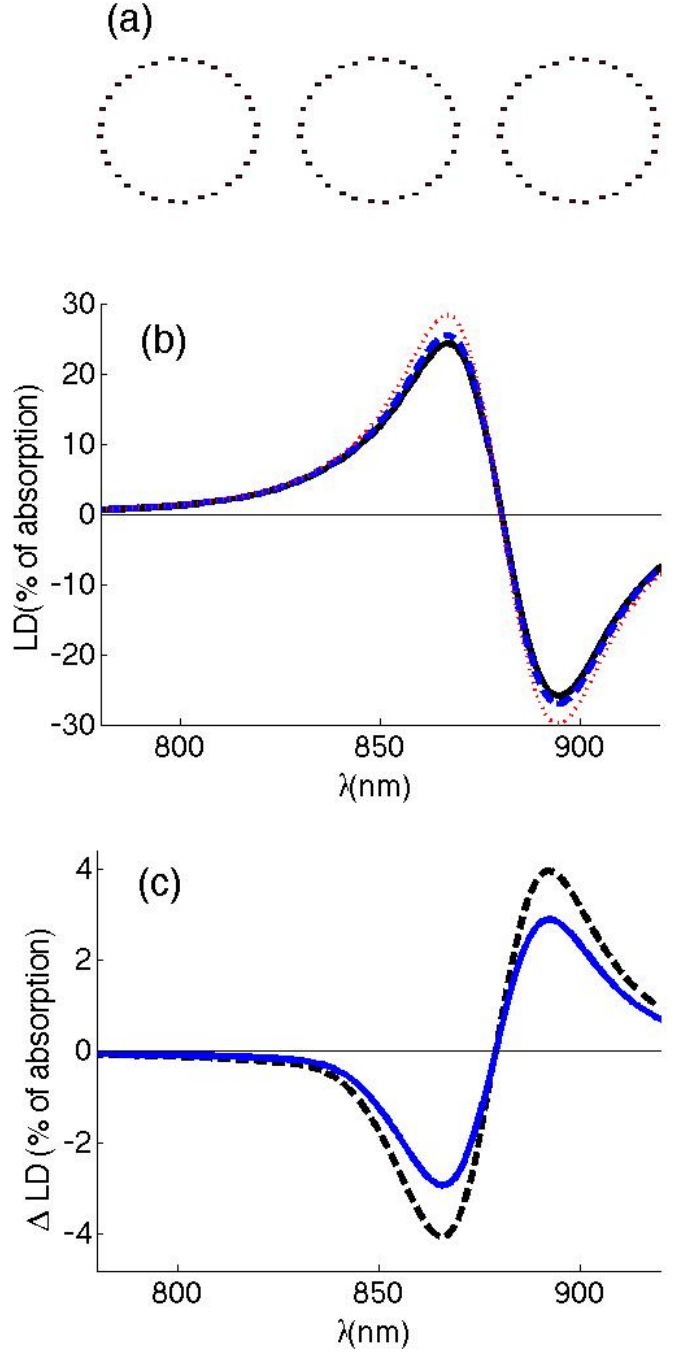


FIG. 10. Linear dichroism in elliptical rings with macromolecular alignment. In (a) configurations studied present a major axes aligned along the direction that connects the linear-like assembly. In (b) the *LD* of these configurations (1, 2 and 3 rings in dotted, dashed and continuous line code) is quite great, but the subtraction among the linear dichroism for 3 rings and 1 rings (dashed), or 2 rings and 1 ring (continuous) leads in (c) to different ΔLD which resemble the signal obtained from circular complexes. Eccentricity of the rings is 0.4, results from average of 3×10^4 realisations of inhomogenous noise.